

Electric bias control of impurity effects in bilayer graphene

Y. G. Pogorelov,¹ M. C. Santos,² and V. M. Loktev^{3,4}

¹*IFIMUP-IN, Departamento de Física, Universidade do Porto, Rua do Campo Alegre 687, Porto 4169-007, Portugal*

²*Departamento de Física, Universidade de Coimbra, R. Larga, Coimbra 3004-535, Portugal*

³*Bogolyubov Institute for Theoretical Physics, NAN of Ukraine, 14b Metrologichna Str., Kiev 03680, Ukraine*

⁴*National Technical University of Ukraine KPI, Pr. Peremogy 37, Kiev 03056, Ukraine*

(Received 15 October 2014; revised manuscript received 26 May 2015; published 3 August 2015)

Formation of localized impurity levels within the band gap in bigraphene under applied electric field and the conditions for their collectivization at finite impurity concentrations are considered. It is shown that a qualitative restructuring of the quasiparticle spectrum within the initial band gap and subsequent metal-insulator phase transitions are possible for such disordered systems, being effectively controlled by variation of the electric field bias. Since these effects can be expected at low enough impurity concentrations and accessible applied voltages, they can be promising for practical applications in nanoelectronics devices.

DOI: [10.1103/PhysRevB.92.075401](https://doi.org/10.1103/PhysRevB.92.075401)

PACS number(s): 74.70.Xa, 74.62.-c, 74.62.Dh, 74.62.En

I. INTRODUCTION

Between various derivatives from the basic graphene system [1–3], special interest is attributed to its bilayer combination [4]. This interest is mainly due to the important possibility of realizing here a semiconductor with a controllable band gap through the application of an electric field normal to the layers [5–8]. It should be noted that a similar crystalline structure of two planes with hexagonal lattices is now recognized for a whole family of materials, either really fabricated or theoretically predicted. Besides the two known modifications of bilayer graphene itself, the Bernal (or A-B) structure [9] and its alternative, the A-A structure [10], there exist also the bilayers of silicene, the silicon analog to graphene [11], the bilayers of boron nitride [12] or its bilayered combination with graphene [13], the bilayered chalcogenides of transition metals (pure or alloyed) [14], etc. However, the most reliable structure for external tuning and rather simple for theoretical study is seen in the Bernal-stacked bilayer graphene, hence chosen here as the basic host system for studying impurity effects. Having introduced impurities in such a system, such as dopants in common semiconductor systems [15,16], there is a possibility for localized impurity levels to appear within the host spectrum gap [17,18]. Next, it is known that, at high enough impurity concentration, an intensive interaction between the localized impurity states related to these levels can take place. This can essentially modify the band spectrum near the gap edge [19,20], giving rise to specific narrow energy ranges of bandlike states near impurity levels (called impurity bands) and even producing a phase transition from insulating to metallic states [21], with important practical applications. An attempt to treat such impurity bands in doped bilayer graphene was done by Nilsson and Castro Neto [17]; however, it missed the crucial issue of whether the respective states in a disordered crystal are really bandlike (extended) or localized and where the separation points between these two kinds in the energy spectrum (the mobility edges [21]) are located. A consistent study of these questions is one of our main purposes here. Having it resolved, the resulting possibility of continuous control on band gap and of controllable phase transitions can make the in-gap impurity states in bilayer graphene quite a flexible tool with regard to electronic properties. A similar situation was recognized

long ago in some magnetic crystals with impurities at the magnon spectra, and so the observable properties can be controlled by an applied magnetic field [22]. Such a possibility for fermionic systems could open interesting possibilities for future nanoelectronics.

The paper is organized as follows. In Sec. II, the second quantization Hamiltonian is defined for a biased Bernal-stacked graphene bilayer (with no impurities) and the related matrix representation for Green's functions (GFs) is built, giving rise to its four-subband electronic spectrum. Section III introduces the model impurity perturbation and analyzes formation of impurity levels and their possible development into impurity bands, based on specific self-energy matrices for the GF matrices. Such impurity bands are considered in more detail in Sec. IV, including the estimates for mobility edges between the bandlike and localized states. Then the possibility for metal-insulator phase transitions in doped bilayer graphene under electric field bias (at fixed impurity concentration) and the resulting transport effects are analyzed in Sec. V. The final Sec. VI presents the main conclusions and suggestions for practical applications of the described impurity effects.

II. BILAYER GRAPHENE UNDER APPLIED FIELD

As is well known, the relevant electronic dynamics of a graphene sheet are generated by the carbon sp^3 orbitals (whose energy level can be chosen as the energy reference) in the simplest approximation of single hopping parameter t between nearest-neighbor carbons from different sublattices at distance a in the honeycomb lattice [2]. The bilayer graphene structure, furthermore, involves the interlayer hopping t_z by vertical links between nearest neighbors from different sublattices (for Bernal stacking) shown in Fig. 1. With an account taken of an electric bias $V = eEd$ between the layers (with the electron charge e , the applied electric field E , and the interlayer spacing d), this defines the tight-binding (Fourier-transformed) Hamiltonian 4×4 matrix [6]:

$$\hat{H}_{\mathbf{k}} = \begin{pmatrix} V/2 & \gamma_{\mathbf{k}} & 0 & t_z \\ \gamma_{\mathbf{k}}^* & V/2 & 0 & 0 \\ 0 & 0 & -V/2 & \gamma_{\mathbf{k}} \\ t_z & 0 & \gamma_{\mathbf{k}}^* & -V/2 \end{pmatrix}. \quad (1)$$

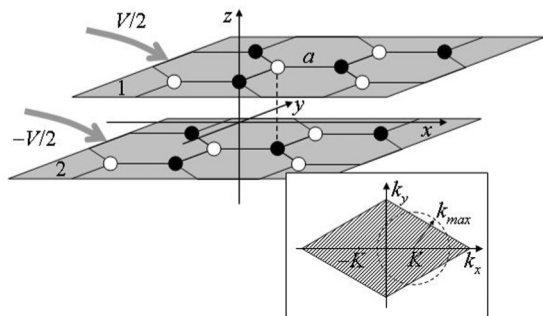


FIG. 1. Schematic of Bernal-stacked bilayer graphene under applied electric bias V . The A- and B-type sites in each plane are indicated by black and white circles, respectively, the solid and dashed lines indicate the in-plane t and interplane t_z links. Inset: the Brillouin zone in \mathbf{k} plane with two Dirac points $\pm\mathbf{K}$ and an equivalent circle of radius $k_{\max} = \sqrt{K/a}$.

Here the wave vector \mathbf{k} lies in the first Brillouin zone (see inset in Fig. 1) and the in-plane dispersion follows from the sums $\gamma_{\mathbf{k}} = t \sum_{\delta} e^{i\mathbf{k}\cdot\delta}$ over nearest-neighbor vectors δ of the honeycomb lattice. It suitably approximates as $\gamma_{\mathbf{k}} \approx \xi_{\mathbf{k}} e^{i\varphi_{\mathbf{k}}}$, with $\xi_{\mathbf{k}} = \hbar v_F |\mathbf{k} - \mathbf{K}|$ near the Dirac points $\mathbf{K} = \pm(4\pi/3\sqrt{3}a, 0)$, where the Fermi velocity $v_F = 3ta/2\hbar$, and $\varphi_{\mathbf{k}} = \arctan k_y/(k_x - K_x)$. The relevant range of $|\mathbf{k} - \mathbf{K}| \sim Kt_z/W$ is really narrow, since t_z is weak besides the total bandwidth W (see below). Then the second-quantization Hamiltonian (in absence of impurity perturbation),

$$H_0 = \sum_{\mathbf{k}} \psi_{\mathbf{k}}^{\dagger} \hat{H}_{\mathbf{k}} \psi_{\mathbf{k}}, \quad (2)$$

involves the spinors $\psi_{\mathbf{k}}^{\dagger} = (a_{1\mathbf{k}}^{\dagger}, b_{1\mathbf{k}}^{\dagger}, a_{2\mathbf{k}}^{\dagger}, b_{2\mathbf{k}}^{\dagger})$ made of Fourier-transformed second quantization operators $a_{j\mathbf{k}} = N^{-1} \sum_{\mathbf{n}} a_{j\mathbf{n}} e^{i\mathbf{k}\cdot\mathbf{n}}$ and $b_{j\mathbf{k}} = N^{-1} \sum_{\mathbf{n}} b_{j\mathbf{n}} e^{i\mathbf{k}\cdot\mathbf{n}}$, where the on-site operators $a_{j\mathbf{n}}$ and $b_{j\mathbf{n}}$ relate to A- and B-type sites from n th unit cell in the $j(=1,2)$ th layer, and N is the number of cells in a layer. Generally, the energy spectrum is defined by the matrix of Fourier-transformed two-time GFs [23,24] $\hat{G}_{\mathbf{k}} = \langle\langle \psi_{\mathbf{k}} | \psi_{\mathbf{k}}^{\dagger} \rangle\rangle$ as solutions of the dispersion equation:

$$\text{Re det } \hat{G}_{\mathbf{k}}^{-1} = 0. \quad (3)$$

Thus for the nonperturbed system by Eq. (2), the GF matrix reads $\hat{G}_{\mathbf{k}}^{(0)} = (\varepsilon - \hat{H}_{\mathbf{k}})^{-1}$ and, after diagonalization of $\hat{H}_{\mathbf{k}}$ in spinor indices, its dispersion near the Dirac points is suitably expressed through the radial variable $\xi_{\mathbf{k}} \equiv \xi$. It includes two positive energy subbands [6],

$$\varepsilon_{\nu}(\xi) = \sqrt{\frac{t_z^2}{2} + \frac{V^2}{4} + \xi^2 - (-1)^{\nu} \sqrt{\frac{t_z^4}{4} + \xi^2(t_z^2 + V^2)}}, \quad (4)$$

the ‘‘external’’ ($\nu = 1$) and ‘‘internal’’ ($\nu = 2$) ones, and their negative energy counterparts, as shown in Fig. 2(a). The most relevant feature of this spectrum is the bias-controlled energy gap between the extrema $\pm\varepsilon_g = \pm V/[2\sqrt{1 + (V/t_z)^2}]$ of two internal subbands, attained along a circle around each Dirac point (the so-called Mexican hat) whose radius in the ξ variable is $\xi_0 = \sqrt{\varepsilon_g^2 + V^2/4}$.

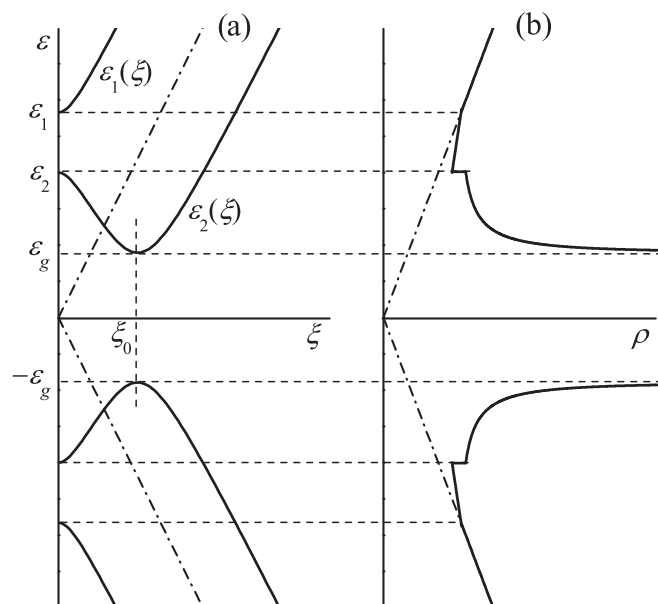


FIG. 2. (a) Dispersion laws for the bilayer in Fig. 1 vs the radial variable ξ near a Dirac point, given by Eq. (4) at the choice of $V = 2t_z$; the dash-dotted line indicate the Dirac dispersion for monolayered graphene. (b) DOS for this choice; the dash-dotted line marks the linear DOS for monolayered graphene.

The GF matrix generates physical characteristics of this system as, for instance, the density of states (DOS) of electronic quasiparticles,

$$\rho(\varepsilon) = \frac{1}{\pi} \text{Im Tr } \hat{G}(\varepsilon), \quad (5)$$

where $\hat{G}(\varepsilon) = (2N)^{-1} \sum_{\mathbf{k}} \hat{G}_{\mathbf{k}}(\varepsilon)$ is the local GF matrix, and its imaginary part for exact band spectrum results usually from an infinitesimal imaginary shift of energy argument, $\varepsilon - i0$ [24]. In what follows, the sum in \mathbf{k} over triangular halves of the Brillouin zone is approximated by the ξ integration,

$$\frac{1}{2N} \sum_{\mathbf{k}} f_{\mathbf{k}}(\varepsilon) \approx \frac{2}{W^2} \int_0^W f(\xi, \varepsilon) \xi d\xi,$$

over two equivalent circles around the Dirac points (inset in Fig. 1) of the ξ radius $W = \hbar v_F k_{\max}$ (where $k_{\max} = \sqrt{K/a}$, see inset in Fig. 1). This approximation is well justified at low energies, $|\varepsilon| \ll W$, compared to the effective bandwidth W . For the pure bilayer graphene system by Eq. (1), the result for Eq. (5) is generated by the explicit diagonal elements of the nonperturbed local GF matrix [17]:

$$\begin{aligned} G_{11}^{(0)} &\approx 2 \frac{\varepsilon - \varepsilon_2}{W^2} \left[\frac{\varepsilon \varepsilon_2}{\delta^2} \left(\pi - \arctan \frac{\delta^2}{\varepsilon^2 + \varepsilon_2^2} \right) + \ln \frac{\gamma}{W} \right], \\ G_{22}^{(0)} &= G_{11}^{(0)}(\varepsilon) - t_z^2 \frac{\varepsilon + \varepsilon_2}{W^2 \delta^2} \left(\pi - \arctan \frac{\delta^2}{\varepsilon^2 + \varepsilon_2^2} \right), \end{aligned} \quad (6)$$

where

$$\begin{aligned} \delta^2(\varepsilon) &= \sqrt{(t_z^2 + V^2)(\varepsilon_g^2 - \varepsilon^2)}, \\ \gamma^2(\varepsilon) &= \sqrt{(\varepsilon^2 - \varepsilon_1^2)(\varepsilon^2 - \varepsilon_2^2)}. \end{aligned}$$

These elements reveal the inverse square root divergences at the gap edges $\pm\varepsilon_g$ (of $\text{Im } G$ beyond the gap and of $\text{Re } G$ within the gap); also note the finite steps of $\text{Im } G$ at the limiting energies $\varepsilon_{1,2} \equiv \varepsilon_{1,2}(0)$ of the two subbands. The resting diagonal elements are simply $G_{33}^{(0)}(\varepsilon) = -G_{22}^{(0)}(-\varepsilon)$ and $G_{44}^{(0)}(\varepsilon) = -G_{11}^{(0)}(-\varepsilon)$, so that finally DOS is a function of ε^2 , as shown in Fig. 2(b), in agreement with the known previous calculations [8]. It presents BCS-like divergences near ε_g^2 , finite steps at $\varepsilon_{1,2}^2$, and coincides with the linear DOS for monolayer graphene [2,3] beyond ε_1^2 due to joint (nonlinear) contributions from both subbands.

Within the gap, only real parts of $G_{jj}(\varepsilon)$ are nonzero, and their divergences near the gap edges are crucial for appearance, under the effect of localized impurity perturbations, of in-gap localized levels, and related collective states, which is the main focus for the analysis below.

III. IMPURITY LEVELS AND IMPURITY SUBBANDS

As was recognized from experimental studies of graphene systems [25], they can contain a variety of defects, ranging from topological ones (vacancies, dislocations, edges, boundaries, etc.) to impurity adatoms (or some functional groups) near one of the planes and in-plane substitutes or interstitials. This provides a doping of charge carriers (of both signs) into these systems, as well as scattering of carriers on impurity potentials and possibly formation of localized (or resonance) impurity states on such potentials. The latter must be characterized by some model parameters within the common tight-binding approximation, and the simplest case is the Lifshitz model, involving only the on-site perturbation potential U , identical for all impurity sites randomly distributed among the lattice sites [26]. This model was already used in the literature on impurity problems in graphene systems, with U values ranging from the Born regime, $|U| \ll W$ [17,27,28], to the unitary limit, $|U| \gg W$ [28,29]. For the case of substitutional impurities in graphene, this value can be roughly estimated by the differences between the first ionization potential of 11.26 V for C and those for its neighbors in the periodic table: 8.3 V for B and 14.53 V for N. Then, for the commonly adopted graphene bandwidth of $W \approx 7$ eV, the choice of $|U|/W \sim 1/2$ looks to be plausible. Also, for diluted impurities at separations much greater than the screening radius [27], the Lifshitz model looks more adequate than the alternative choice of the Anderson model [30], with random perturbations at each lattice site in Ref. [31]. Another alternative is the Anderson hybrid (or s - d) model [32] with two parameters, the impurity binding energy and its coupling to the host excitations. Its use for the so-called deep impurity levels in semiconductors is known to result in formation of the above-mentioned impurity bands and related phase transitions [19]. However, such a perturbation model, when introduced into the framework of a four-component host spectrum of Sec. II, could make the treatment of interactions between impurities and of impurity band coherence technically unfeasible. This determines our choice for the Lifshitz model (though known to provide less freedom for impurity band formation than the s - d model). Due to similar reasons, we do not consider the long-range Coulomb impurity potentials [33,34].

Let us build the perturbation Hamiltonian by Lifshitz impurities on certain impurity sites. In accordance with the composition of ψ spinors, the A and B sites from the first plane can be referred to the types $j = 1, 2$, respectively, and those from the second plane to $j = 3, 4$, and then \mathbf{p}_j denotes the defect sites of j th type with relative concentrations $c_j = \sum_{\mathbf{p}_j} N^{-1}$ such that the total impurity concentration $\sum_j c_j = c \ll 1$. Then the sought Hamiltonian in terms of local Fermi operators reads

$$H_1 = U \left(\sum_{\mathbf{p}_1} a_{1\mathbf{p}_1}^\dagger a_{1\mathbf{p}_1} + \sum_{\mathbf{p}_2} b_{1\mathbf{p}_2}^\dagger b_{1\mathbf{p}_2} + \sum_{\mathbf{p}_3} a_{2\mathbf{p}_3}^\dagger a_{2\mathbf{p}_3} + \sum_{\mathbf{p}_4} b_{2\mathbf{p}_4}^\dagger b_{2\mathbf{p}_4} \right), \quad (7)$$

or, in terms of ψ spinors by Eq. (2), it takes the form of a scattering operator,

$$H_1 = \frac{1}{N} \sum_{j, \mathbf{p}_j} \sum_{\mathbf{k}, \mathbf{k}'} e^{i(\mathbf{k}' - \mathbf{k}) \cdot \mathbf{p}_j} \psi_{\mathbf{k}}^\dagger \hat{U}_j \psi_{\mathbf{k}'}, \quad (8)$$

where the diagonal matrix \hat{U}_j has a single nonzero element U at the jj site. Considering now the Hamiltonian in the presence of impurities $H_0 + H_1$ and following a similar routine to Ref. [35], we arrive at solutions for the GF matrix in two specific forms adequate for two alternative types of excitation states in a disordered system [21,26]: the bandlike (extended) states and localized states. Thus, the first of these types is better described by the so-called fully renormalized representation (FR) of GF [22],

$$\hat{G}_{\mathbf{k}} = [((\hat{G}_{\mathbf{k}}^{(0)})^{-1} - \hat{\Sigma}_{\mathbf{k}})]^{-1}, \quad (9)$$

providing the roots of the dispersion equation [Eq. (3)], classified along the quasimomentum \mathbf{k} . Here the self-energy matrix is additive in different types of impurity centers: $\hat{\Sigma}_{\mathbf{k}} = \sum_j \hat{\Sigma}_{j, \mathbf{k}}$, with the partial matrices given by the related FR group expansions (GEs) in complexes of impurity centers (of the same j type, involved in multiple scattering processes):

$$\hat{\Sigma}_{j, \mathbf{k}} = c_j \hat{T}_j \left[1 + c_j \sum_{\mathbf{n} \neq 0} (e^{-i\mathbf{k} \cdot \mathbf{n}} \hat{A}_{j, \mathbf{n}} + \hat{A}_{j, \mathbf{n}} \hat{A}_{j, -\mathbf{n}}) \times (1 - \hat{A}_{j, \mathbf{n}} \hat{A}_{j, -\mathbf{n}})^{-1} + \dots \right]. \quad (10)$$

Each T matrix $\hat{T}_j = \hat{U}_j (1 - \hat{G} \hat{U}_j)^{-1}$ describes all the scatterings on a single impurity center of j th type, and the next-to-unity term in the right-hand side of Eq. (10) accounts for scatterings on pairs of j impurities through the matrices $\hat{A}_{j, \mathbf{n}} = \hat{T}_j (2N)^{-1} \sum_{\mathbf{k}' \neq \mathbf{k}} \hat{G}_{\mathbf{k}'} e^{i\mathbf{k}' \cdot \mathbf{n}}$ of indirect interaction (via bandlike excitations) in such pairs at separation \mathbf{n} . Notice the excluded quasimomentum \mathbf{k} (for given $\hat{\Sigma}_{\mathbf{k}}$) in this sum; also the FR GE excludes coinciding quasimomenta in all the multiple sums for products of interaction matrices [22]. The omitted terms in Eq. (10) relate to all scattering processes in groups of three and more impurities, and their general structure can be found in similarity with the known group integrals from the Ursell-Mayer classical theory of nonideal gases.

Otherwise, for the range of localized states, the nonrenormalized representation (NR),

$$\hat{G}_{\mathbf{k}} = \hat{G}_{\mathbf{k}}^{(0)} - \hat{G}_{\mathbf{k}}^{(0)} \hat{\Sigma} \hat{G}_{\mathbf{k}}^{(0)}, \quad (11)$$

defining rather DOS from Eq. (5) than dispersion from Eq. (3), is more adequate. Here the respective NR self-energy matrix $\hat{\Sigma} = \sum_j \hat{\Sigma}_j$ has a similar structure to the FR structure by Eq. (10) but with the NR matrices $\hat{T}_j^{(0)} = \hat{U}_j(1 - \hat{G}^{(0)}\hat{U}_j)^{-1}$, $\hat{G}^{(0)} = (2N)^{-1} \sum_{\mathbf{k}} \hat{G}_{\mathbf{k}}^{(0)}$, and with no restrictions in all the quasimomentum sums for the products of NR interaction matrices $\hat{A}_{j,n}^{(0)} = \hat{T}_j^{(0)}(2N)^{-1} \sum_{\mathbf{k}} \hat{G}_{\mathbf{k}}^{(0)} e^{i\mathbf{k}\cdot\mathbf{n}}$ (that are only present in their even combinations $\hat{A}_{j,n}^{(0)}\hat{A}_{j,-n}^{(0)}$).

The best-known effect of local perturbations consists in emergence of localized energy levels within the band gap, and those were already indicated for impurities in bilayer graphene [17,18]. As known from general theory [22,26], such levels are most pronounced at sufficiently low concentration of impurities (so that their indirect interactions can be neglected) when they are given by the poles of T matrices. In the present case, the matrices $\hat{T}_j^{(0)}$ give rise to four different local levels $\varepsilon^{(j)}$ within the band gap, and their locations depend on the magnitude and sign of perturbation parameter U (like the known situations in common doped semiconductors [15,16]) but yet on the applied field V (as a specific of doped bilayer graphene). The positions of four impurity levels $\varepsilon^{(j)}$ by each type of impurity center are the roots of related Lifshitz equations,

$$UG_{jj}^{(0)}(\varepsilon^{(j)}) = 1, \quad (12)$$

so that choosing for definiteness $U = -W/2$ and using Eq. (6) provides their dependence on the applied bias V as shown in Fig. 3 (for their relative separations from the gap edge). It is seen that generally they stay rather shallow at growing V ,

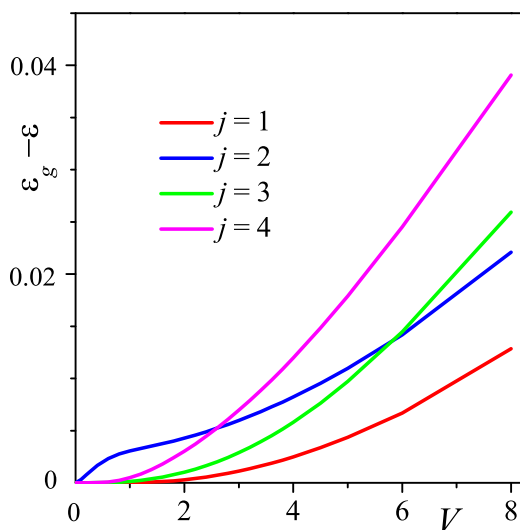


FIG. 3. (Color online) Separations of the in-gap impurity levels $\varepsilon^{(j)}$ from the gap edge as functions of the applied bias V (all in t_z units) for the choice of impurity perturbation parameter $U = -W/2$. Note the different behaviors of $\varepsilon^{(1,2)}$ and $\varepsilon^{(3,4)}$ pairs and the interchange of the deepest level from $\varepsilon^{(2)}$ to $\varepsilon^{(4)}$ at the bias value $V_{cr} \approx 2.6t_z$ (see also the text).

but with a notable difference between the levels $\varepsilon^{(1,2)}$ (by impurities in the positive biased layer) and $\varepsilon^{(3,4)}$ (by those in the negative biased layer). In particular, a specific interchange of the deepest levels occurs in this course, from $\varepsilon^{(2)}$ to $\varepsilon^{(4)}$, at $V_{cr} \approx 2.6t_z$ for the given U . This feature was not indicated in the former analysis of the same model in Ref. [17] where only $\varepsilon^{(2)}$ was considered as the deepest level. However, for the commonly used value of $t_z \approx 0.35$ eV, this interchange bias would amount to $V_{cr} \approx 0.91$ eV, well above the experimentally realized (to the moment) V values of up to ≈ 0.36 eV [5]. Thus, the much stronger separation of the $\varepsilon^{(2)}$ level at lower bias voltages could be of more practical importance.

Also, we note that while the impurity levels generally become deeper at greater U values, the indicated interchange bias decreases in this course: from $V_{cr} \approx 3.53t_z$ at $U = -W/4$ to $V_{cr} \approx 1.88t_z$ at $U = -W$.

The well-known property of localized states by shallow energy levels is their long effective radius [22], also indicated for impurities in biased bilayer graphene [17], defining intensive interactions between them already at their very low concentrations. Such interactions were shown to allow, at certain conditions, collectivization of impurity states to form specific bandlike states within narrow energy bands (called impurity bands) around the initial localized levels [19]. As will be seen below, this effect is possible as well in the present case of multiple localized levels, where the most essential specifics is their joint participation in forming the lowest impurity subband of much stronger dispersion than in higher-lying subbands (if those are permitted).

Formally, in similarity to the nonperturbed case, the band spectrum for the disordered system can be evaluated from the dispersion equation, Eq. (3), with the FR GF matrix by Eqs. (9) and (10). Of course, if treated rigorously, it presents a tremendous problem of developing an infinite sequence of renormalization procedures in all possible terms of the corresponding GE, and there is no reasonable hope for its exact solution. On the other hand, validity of the relatively simpler NR, Eq. (11), is only limited to the energy ranges of localized states.

One could try to use the coherent potential approximation (CPA) [36], a useful tool, e.g., in the theory of disordered alloys, where the full self-energy is presented in a self-consistent T-matrix form. It reduces the impurity effect at each given energy to a certain spatially uniform potential adjusted to make the average scattering zero. This is done through a stable iterative procedure and readily provides a definite band spectrum. However, this approach treats the disordered system as if keeping unbroken translation symmetry and so leads to a purely extended spectrum, unlike its real composition of bandlike and localized ranges [21]. Therefore the CPA results can be only justified within the bandlike ranges, far enough from their edges [37], accordingly to the known Ioffe-Regel-Mott (IRM) criterion of long enough mean free path compared to the wavelength [21,38]. Moreover, for the disorder due to diluted impurities, CPA applies only to the less perturbed interiors of the broad initial bands but *not* to the narrow impurity bands between close mobility edges. This can be verified by comparing its results to those by more consistent theories or to experimental data (when available). The CPA versions were also suggested for impurity effects

both in monolayer graphene [39] and bilayer graphene [17], producing in the latter case some band features within the initial band gap. But our analysis below, starting from the same structure of impurity levels as in Ref. [17], results in a quite different picture of impurity bands and we justify it based on the IRM criteria relevant for this case.

The practical approach to this picture is done through partial renormalizations of the full self-energy in Eq. (10), first substituting there the NR T matrix and interaction matrices and then subsequently introducing such approximate self-energies into the next generations of GF and interaction matrices. In this course, convergence of the obtained GEs is checked in order not to extend the renormalizations to irrelevant GE terms. Namely, it is reasonable to define the l th-generation GF matrix $\hat{G}_{\mathbf{k}}^{(l)}$ by an analog to Eq. (9) with the respective self-energy $\hat{\Sigma}_{\mathbf{k}}^{(l)}$ by an analog to Eq. (10) but containing the matrices $\hat{T}^{(l-1)}$ and $\hat{A}_{\mathbf{n}}^{(l-1)}$ built from the preceding generation $\hat{G}_{\mathbf{k}}^{(l-1)}$ matrices. This algorithm leads to the true FR at $l \rightarrow \infty$. However, even its first nontrivial $l = 1$ approximation can be reasonable for the bandlike energy ranges where the true FR GE converges.

Then, in the first step of this routine, the formal solutions of Eq. (10) with the self-energies in the NR T-matrix approximation, $\hat{\Sigma}_{j,\mathbf{k}} \approx c_j \hat{T}_j^{(0)}$, display four narrow subbands near four impurity levels $\varepsilon^{(j)}$, besides the four broad principal bands $\pm \varepsilon_v(\xi)$ [here only slightly modified compared to Eq. (4)]. An example of such a modified spectrum (at a natural choice of equal partial concentrations $c_j = c$ and taking the total impurity concentration $4c = 0.01$) for the cases of Fig. 3 is shown in Fig. 4. The lowest impurity subband, conventionally denoted here as $\varepsilon^{(2)}(\xi)$ by its proximity to the lowest $\varepsilon^{(2)}$ level, is seen to strongly dominate in its dispersion over all the resting ones, and the direct analysis of Eq. (10) shows that this domination is due to the above-mentioned constructive interplay between all $\varepsilon^{(j)}$.

Note that all the impurity subbands in this approximation produce BCS-like divergences in DOS, as well near the levels $\varepsilon^{(j)}$ as near subband terminations. However, since quasimomentum is not a true quantum number in a disordered system [26], the analysis of its real energy spectrum, especially for the in-gap states, should also take account of the damping $\Gamma_j(\xi)$ of each $\varepsilon^{(j)}(\xi)$ state resulting from $\text{Im} \Sigma_j$. Hence one can consider these states Bloch-like (or conducting) only if the IRM criterion is fulfilled or the GE, Eq. (10), is convergent at related energies. Otherwise they should pertain to the localized type. As will be seen, all the formal DOS singularities fall within the localized energy ranges and so are effectively broadened.

The mentioned criteria also permit one to estimate the Mott mobility edges between the bandlike and localized ranges. Of course, such edges can be found near the limits of both principal and impurity bands, but our main focus here will be on the most dispersive impurity band, for instance, $\varepsilon^{(2)}(\xi)$ in the above example. Finally, a certain special value V_A of bias control (at given impurity concentrations c_j and perturbation parameter U) can be indicated, such that mobility edges from both sides of a conducting impurity band will merge. This collapse of the impurity band will manifest a kind of Anderson transition [30] in a disordered system, realized in a controllable way at $V \rightarrow V_A$.

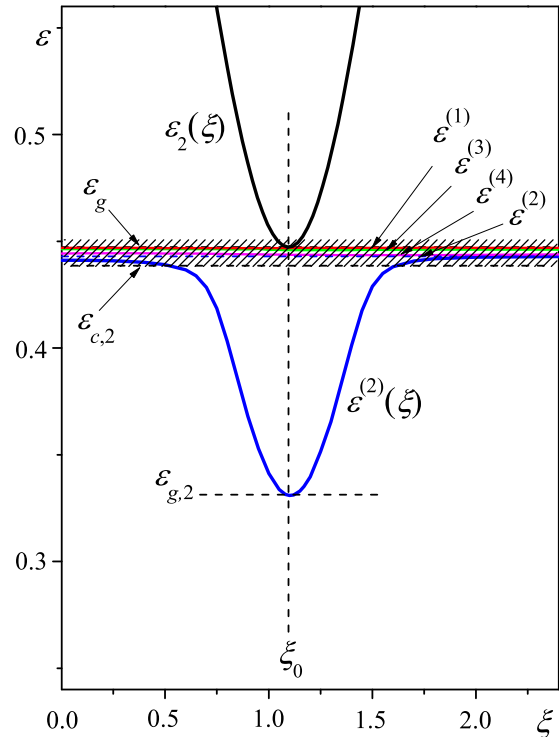


FIG. 4. (Color online) Formation of impurity subbands near the impurity levels by the solutions of Eq. (3) in the first step of renormalization (see text) for the case of Fig. 3 at $V = 2t_z$ and $c = 0.01$ (with the variables ε and ξ presented in t_z units). Only the most dispersive $\varepsilon^{(2)}(\xi)$ subband extends well beyond the shadowed vicinity of the $\varepsilon^{(2)}$ level, which delimits the range of localized states down to the respective mobility edge $\varepsilon_{c,2}$. Together with the localized states around $\varepsilon^{(4,3,1)}$, this range continues up to above the gap edge ε_g .

It should be noted that all these fundamental features of the energy spectrum in a disordered system are lost when the impurity bands are treated within the CPA approximation (as, e.g., in Refs. [17] and [39]).

IV. CONDITIONS FOR THE EXISTENCE OF IMPURITY SUBBANDS

As known from studies on many disordered systems where a localized impurity level ε_{imp} near an edge ε_g of pure crystal energy band can give rise, at high enough impurity concentration, to a specific impurity band $\varepsilon_{\text{imp}}(\mathbf{k})$ [22], the latter is restricted by the general IRM criterion,

$$\mathbf{k} \cdot \nabla_{\mathbf{k}} \varepsilon_{\text{imp}}(\mathbf{k}) \gg \Gamma_{\text{imp}}[\varepsilon_{\text{imp}}(\mathbf{k})], \quad (13)$$

where the linewidth $\Gamma_{\text{imp}}(\varepsilon)$ of a Bloch-like state with quasimomentum \mathbf{k} and energy ε is defined as the imaginary part of the corresponding self-energy. For the present multiband system, this criterion should be formulated for each of the $\varepsilon^{(j)}(\xi)$ subbands by expanding the general determinant from Eq. (3) near a given energy ε in a complex form, $\det \hat{G}_{\mathbf{k}}^{-1} \approx [\varepsilon - \varepsilon^{(j)}(\xi) + i\Gamma_j(\varepsilon)]\Omega_j(\varepsilon)$, to obtain the corresponding linewidth $\Gamma_j(\varepsilon)$ [aside from a certain factor $\Omega_j(\varepsilon)$ of energy-to-cube dimension].

In the adopted Lifshitz model, each partial T matrix \hat{T}_j (regardless of its renormalization) has a single nonzero element at the jj site (alike \hat{U}_j itself): $T_j = U/(1 - UG_{jj})$. For the above suggested first step renormalization, we have $\text{Im}T_j^{(0)} = 0$ for ε within the band gap. Here the imaginary part of related self-energy function $\Sigma_j^{(1)}$ is only due to the GE terms next to unity in Eq. (10), dominated by the pair term once GE is convergent. It can be also shown that the most relevant contribution to $\text{Im}\Sigma_j(\varepsilon)$ comes from the jj th matrix element of the GE pair term, while those from its other elements (though generally nonzero) are strongly reduced by the quantum interference effects. This contribution,

$$B_j(\varepsilon) = \text{Im} \sum_{n>a} \frac{A_{j,\mathbf{n}}^{(0)} A_{j,-\mathbf{n}}^{(0)}}{1 - A_{j,\mathbf{n}}^{(0)} A_{j,-\mathbf{n}}^{(0)}}, \quad (14)$$

can be obtained from the residues at zeros of the denominator, using the explicit spatial behavior of scalar interaction functions (see Appendix for details),

$$\begin{aligned} A_{j,\mathbf{n}}^{(0)}(\varepsilon) &= \frac{T_j^{(0)}(\varepsilon)}{2N} \sum_{\mathbf{k}} e^{i\mathbf{k}\cdot\mathbf{n}} (G_{\mathbf{k}}^{(0)})_{jj} \\ &\approx \sqrt{\frac{r_{j,\varepsilon}}{n}} e^{-n/r_{j,\varepsilon}} \sin \frac{n}{r_0} \cos \mathbf{K} \cdot \mathbf{n}, \end{aligned} \quad (15)$$

where the characteristic scales are

$$r_{j,\varepsilon} = r_0 \left(\pi \frac{\varepsilon_g - \varepsilon^{(j)}}{\varepsilon - \varepsilon^{(j)}} \right)^2, \quad r_\varepsilon = r_0 \frac{\xi_0^2}{\delta^2}, \quad r_0 = \frac{\hbar v_F}{\xi_0}.$$

A similar behavior with two oscillating factors in effective interimpurity interactions was previously indicated for the impurity states within a superconducting gap in iron pnictides [35], where a faster cosine factor had Fermi wavelength. But the present case is simplified by the \mathbf{K} -point specific property that, for all separations \mathbf{n} between lattice sites of the same j th type, $\cos^2 \mathbf{K} \cdot \mathbf{n}$ only takes the values $\sigma = 1$ and $1/4$ (with respective weights $p_\sigma = 1/3$ and $2/3$), whose contributions can be then simply added up in Eq. (14). These partial contributions are obtained by subsequent integrations [35], first over the poles of fast oscillating sine and then over its residues with the slow envelope function $F_{j,n,\sigma}^2 = \sigma r_{j,\varepsilon} e^{-2n/r_{j,\varepsilon}}/n$:

$$\begin{aligned} B_j &= \sum_{\sigma} p_{\sigma} \text{Im} \sum_{n>a} \frac{F_{j,n,\sigma}^2 \sin^2(n/r_0)}{1 - F_{j,n,\sigma}^2 \sin^2(n/r_0)} \\ &\approx \sum_{\sigma} \frac{4\pi p_{\sigma}}{\sqrt{3}a^2} \int_a^{r_{\max}} \frac{r dr}{\sqrt{F_{j,r,\sigma}^2 - 1}}, \end{aligned} \quad (16)$$

where r_{\max} corresponds to $F_{j,r_{\max}} = 1$. The latter integration is simplified within the energy range of

$$\varepsilon^{(j)} - \varepsilon \gg (\varepsilon_g - \varepsilon^{(j)})^{5/4} / \varepsilon_g^{1/4}, \quad (17)$$

where $r_{j,\varepsilon} \ll r_\varepsilon$ so that the exponential factor in Eq. (15) is approximately unity for all $r < r_{\max} \approx r_{j,\varepsilon}$. In this approximation, the explicit result for the most dispersive subband reads

$$B_2(\varepsilon) = \frac{7\pi}{64} \left(\frac{r_{2,\varepsilon}}{a} \right)^2, \quad (18)$$

with the prefactor resulting precisely from weighting of σ values. Then the above-suggested expansion of $\det \hat{G}_{\mathbf{k}}^{-1}$ for ε closer to $\varepsilon^{(2)}$ than to other $\varepsilon^{(j)}$ (so that all Σ_j except Σ_2 can be neglected) provides the linewidth,

$$\Gamma_2(\varepsilon) \approx c^2 (\varepsilon^{(2)} - \varepsilon) B_2(\varepsilon), \quad (19)$$

valid until $\varepsilon^{(2)} - \varepsilon \lesssim \varepsilon_g - \varepsilon^{(2)}$. Upon going farther from $\varepsilon^{(2)}$, we have $r_{j,\varepsilon} < r_0$ so that $B_2(\varepsilon)$ vanishes and finite Γ_2 values can only result from the higher-order GE terms (if not to include, of course, such relaxation processes as by thermal phonons, electron-electron collisions, etc.). From Eq. (19), the IRM criterion is reduced to the inequality

$$c B_2(\varepsilon) \ll 1$$

(agreeing with the GE convergence), and, supposing Eq. (17) to be valid, this criterion permits one to estimate the mobility edge separation from the $\varepsilon^{(2)}$ level:

$$\varepsilon^{(2)} - \varepsilon_{c,2} \sim c^{1/4} \sqrt{\frac{W}{2\xi_0}} (\varepsilon_g - \varepsilon^{(2)}). \quad (20)$$

All the states with energies closer to $\varepsilon^{(2)}$ than $\varepsilon_{c,2}$ are localized on certain clusters of second-type impurity centers. The first conclusion from the estimate, Eq. (20), is that existence of the impurity subband itself is only assured if its bandwidth $\approx \varepsilon^{(2)} - \varepsilon_{g,2}$ surpasses the width of localized range around $\varepsilon^{(2)}$. This is fulfilled when the total impurity concentration exceeds the critical value:

$$\begin{aligned} c_{cr} &\sim \left(\frac{t_z}{W} \right)^{8/3} \left(\frac{|U|}{W} \right)^{4/3} \left(\frac{V}{W} \right)^{2/3} \\ &\times \frac{(t_z + \sqrt{t_z^2 + V^2})(2t_z^2 + V^2)}{(t_z^2 + V^2)^{2/3} t_z^{5/3}}. \end{aligned} \quad (21)$$

[It is obtained by approximating Eq. (6) only to its diverging terms.] Smallness of this expression is mainly due to its first three essential factors of interlayer coupling, impurity perturbation, and applied bias, while the last factor stays almost constant for all realistic (not-too-high) V values. Thus, for the sample choice of $W = 20t_z$, $|U| = 10t_z$, and $V = 2t_z$, we obtain $c_{cr} \sim 1.8 \times 10^{-5}$. Then for the example of $c = 0.01$ chosen in Fig. 3, the mobility edge $\varepsilon_{c,2}$ extends from $\varepsilon^{(2)}$ to about the distance $\varepsilon_g - \varepsilon^{(2)}$, while the dispersion of $\varepsilon^{(2)}$ subband is about an order of magnitude bigger (see Fig. 4). Finally, from comparison of ranges by Eqs. (20) and (17), it follows that the latter one for $c > c_{cr}$ always occurs within the localized range and so the exponential factor in Eq. (15) cannot influence the above-obtained estimates. In summary, only the most dispersive impurity subband by the lowest impurity level can be considered to really emerge beyond its mobility edge. Its main specifics is in anomalously strong variation of the lifetimes $\tau(\varepsilon)$ along very narrow energy intervals. As to other formal solutions of Eq. (3) (analyzed with inclusion of the resting B_j), they are mostly invalidated within the common overlapped range of localized levels that extends up to $\varepsilon_{c,+}$, the mobility edge of the upper main band. The states in this area can be characterized only by their DOS. Though the latter function cannot be directly found here from the above-defined GEs [Eqs. (9) and (11)], it can be plausibly expected to vary

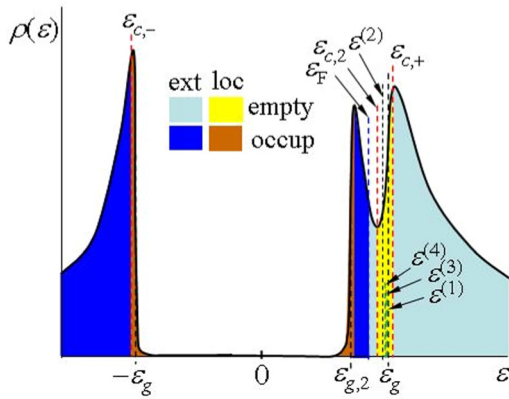


FIG. 5. (Color online) Schematics of extended (ext) and localized (loc) ranges in the energy spectrum of bilayer graphene with impurities for the situation like that of Fig. 4. Note the position of the Fermi level ε_F (separating occupied and empty states) with respect to the mobility edges (separating ext and loc states); the narrow impurity band emerges below only the lowest impurity level $\varepsilon^{(2)}$, while the resting $\varepsilon^{(j)}$ levels get buried within the localized range from $\varepsilon_{c,2}$ up to $\varepsilon_{c,+}$ (see text).

smoothly up to the peak near ε_g (Fig. 5) so that the total number of states $\int_{-W}^W \rho(\varepsilon) d\varepsilon = 4$ is kept.

Similarly, some finer details of the energy spectrum can be found, as, for instance, the rest of the mobility edges $\varepsilon_{c,\pm}$ that define the broadened edges of main subbands, and those near the extremum $\varepsilon_{g,2} \approx \varepsilon^{(2)}(\xi_0)$ of the impurity subband (see Fig. 5). Finally, the case of low impurity concentration, $c < c_{cr}$, can be also considered when there is no impurity band within the gap, but the localized levels $\varepsilon^{(j)}$ turn to be separately resolved. Since all these data are less relevant for our main practical purpose below, they are left beyond the present scope. Nevertheless, the presented results essentially develop the general picture of quasiparticle spectra in crystals with impurities under external fields [22].

V. BIASED METAL-INSULATOR TRANSITIONS AND THEIR OBSERVABLE EFFECTS

Now we can pass to the important processes of electric transport in the system with the above-described band spectrum. For simplicity, this consideration is restricted to the case of zero temperature, and the main attention is paid to the position of Fermi level ε_F and to the lifetime τ_F of Fermi states under the applied bias control V at given parameters of impurity perturbations c and U . The basic condition for the Fermi level,

$$2 \int_{-\infty}^{\varepsilon_F} \rho(\varepsilon) d\varepsilon = 1 + c', \quad (22)$$

defines its shift from the zero energy position in the unperturbed system, in order to accommodate the total of c' extra carriers per unit cell (brought by impurities themselves and possibly by some external sources). This generally requires knowledge of DOS functions for all the impurity subbands (besides weakly perturbed main subbands). But our main interest here is in finding a possibility for ε_F to be located within the most dispersive impurity band $\varepsilon^{(2)}(\xi)$, so we focus on the

related DOS, especially in proximity to this band termination $\varepsilon_{g,2}$ (Fig. 5). An important simplification of this task is obtained by noting that for this energy range all the self-energies Σ_j in Eq. (10) can be taken as constants, small enough compared to the gap width; thus the solutions of the dispersion equation [Eq. (3)] almost reproduce here the nonperturbed $\varepsilon_2(\xi)$ band within accuracy to a constant shift of its edge from ε_g to $\varepsilon_{g,2}$ (see also Fig. 4), just due to the common effect of all Σ_j . The resulting DOS function,

$$\rho_2(\varepsilon) \approx \frac{2\varepsilon}{W^2} \frac{t_z^2 + V^2}{\delta^2}, \quad (23)$$

at $0 < \varepsilon - \varepsilon_{g,2} \lesssim \varepsilon^{(2)} - \varepsilon_{g,2}$ defines from Eq. (21) the Fermi level ε_F position by the equation

$$c' \approx \left(\frac{2}{W}\right)^2 \sqrt{(t_z^2 + V^2)(\varepsilon_g^2 - \varepsilon_F^2)}. \quad (24)$$

Let c'_{\max} be the maximum permitted amount of carriers such that ε_F stays within the conducting range. Then, for the case of Fig. 4, this value results in $c'_{\max} \approx 4 \times 10^{-3}$, that is, somewhat lower than the proper impurity concentration, $c = 10^{-2}$ in this case. Nevertheless, conduction through the impurity band can be realized if c' is brought below the indicated limit of c'_{\max} , e.g., by external compensation of a part of the charge carriers [16]. Once this is assured, one can then strongly change the conductivity by raising the applied V , since the localized range width by Eq. (19) grows with bias faster than $\propto V^{2/3}$ against the almost bias-insensitive (at $V \lesssim V_{cr}$) width of the impurity band, while the Fermi level ε_F goes to the band edge $\varepsilon_{g,2}$ slower than $\propto V^{-2}$. Then the faster advancing mobility edge $\varepsilon_{c,2}$ will finally cross ε_F at some bias V_{M-I} , giving rise to a Mott metal-insulator transition and vanishing conductivity. Thus, for the proposed choice of $U = -W/2 = -10t_z$ and $c' = 3 \times 10^{-3}$, we obtain $V_{M-I} \approx 0.87$ eV. In this course, at $V \rightarrow V_{M-I}$, conductivity can vary by orders of magnitude, when we drive the Fermi inverse lifetime $\tau_F^{-1} \sim \Gamma_2(\varepsilon_F)/\hbar$ close to divergence, under very tiny variations (say, some meV) of bias. This indicates a tremendous potentiality of such types of doped semiconducting systems in comparison with traditional materials.

Besides their evident field transistor applications, critical effects by the biased Mott transition can be also expected in other observable properties of this doped system, for instance, in its optical response at the frequency $\omega_{i,b} \approx (\varepsilon^{(2)} + \varepsilon_g)/\hbar$ of transition from the top of the occupied $-\varepsilon_2(\xi)$ band and the Fermi states of impurity $\varepsilon^{(2)}(\xi)$ band (like the case formerly considered by the authors for doped superconducting iron pnictides [35]), which can be switched on and off by tiny variations of the bias.

At last, with further growing bias, the collapse of upper and lower mobility edges within the impurity band and the aforementioned Anderson transition to a fully localized in-gap spectrum can be realized. From Eq. (20) at $V \lesssim t_z$, this bias value estimates as $V_A \sim c^{3/2} W^7 |U|^{-2} t_z^{-4}$, though this analytic expression applies only (at moderate $|U|$) for as low impurity concentrations as $c \lesssim 10^{-5}$. However, a numerical analysis with use of the full Eq. (6) shows that V_A remains attainable up to $c \sim 10^{-2}$ as well. This transition can also produce observable effects; in this case the collapse of a narrow

impurity band would lead to a dramatic drop of the plasmonic resonance frequency [40].

VI. DISCUSSION AND CONCLUSIONS

The above main conclusion regarding the possibility of attaining extensive control of electrical conduction through very slight variations of applied potential implies, of course, many additional factors to be taken into account. They can be indicated both from the fundamental and practical sides. Thus, the theoretical approach used is restricted to a simple model of impurity perturbation by a single on-site parameter, and some elaboration of it could be done involving, for instance, perturbations of hopping parameters. These kinds of analyses are known for traditional doped semiconductors and also have demonstrated possibilities for similar impurity bands near localized impurity levels at high enough impurity concentrations. Notably, for those materials, the Lifshitz perturbation model was found to be the most restrictive for such effects, for instance, due to unrealistically high critical concentrations, of the order of unity or even more [unlike that in Eq. (19)]. This permits the expectation that modifications of the present Lifshitz model, as in Ref. [18] for single impurities at a gapless spectrum, or using the Anderson hybrid model [32] as in Ref. [41] (provided all the technical aspects be assured), will not essentially change the physical behavior of the system. On the other hand, there are yet many properties of this simple model that can be further studied, for instance, the possibilities to realize multiple conducting impurity subbands and subsequent processes of multiple switching between them, including, e.g., optical transitions under electrical biasing. Of course, a more realistic approach should also take account of topological defects (see the beginning of Sec. III) as well as the above-mentioned Coulombic interactions, thermal effects, etc. Generally, this would require the impurity band structure to exceed a certain “background” relaxation level that could be achieved by varying either the impurity sort (that is, U parameter) and concentration and/or the applied bias V . Finally, similar impurity multiband effects can be also sought in other atomically multilayered systems, such as those mentioned in the Introduction, where a special focus might be put on the tuned band gap in silicene bilayers (yet wider than in bilayer graphene [11]), or even on single layers of buckled silicene or germanene [42].

As to the practical issues, first of all, rather strict conditions on fabrication of the basic doped bilayered system are in order, perhaps mainly aimed to minimize all the “foreign” defects vs the chosen dopants, but the next requirement to control the levels of dopants (and possibly their compensating species) within fractions of percent should not be a real problem for modern nanoelectronics. Special attention is also required for precise control and manipulation of the applied bias V , particularly in exploring possibilities to realize its near-critical and supercritical regimes, like those indicated in the above analysis. Finally, the practical arrangement of an experimental transistor-type setup based on the suggested conductivity control by tiny impurity subbands would perhaps require some specific technical solutions. However, they do not look too difficult to be found in the available engineering

depository. Thus a fair hope exists for this theoretical proposal to be realized in a practical device.

In conclusion, the effects of localized on-site perturbations by rather disperse impurities on a bilayered graphene system under applied electrical bias between the layers are analytically considered using the Green’s function techniques adapted for a multiband electronic system. Thus the conditions for different types of localized impurity levels to appear within the bias-induced band gap in the electronic spectrum of this system and then for extension of these levels into specific narrow energy bands at impurity concentrations above certain characteristic values are demonstrated. The analysis of these processes demonstrated their similarities to those known from literature on various crystalline materials with impurities. Also, some specifics of the present system were shown in considerable bias dependencies of impurity bands and of critical concentrations for their formation. These dependencies can be further treated to provide some specific phase diagrams in variable “bias concentrations,” as they occurred in antiferromagnetic insulators where such diagrams in variable “magnetic field concentrations” were quite informative [22]. A practical application of the described electronic band structure is suggested in a form of highly sensitive bias control of the system’s conductivity through the impurity subband when brought close to a regime of bias-controlled Mott metal-insulator transition.

ACKNOWLEDGMENTS

Y.G.P. is grateful for the support of this work from the Portuguese FCT, Project No. PTDC/FIS/120055/2010, and M.C.S. is indebted to the FCT for support from Project No. PTDC/QUI-QUI/117439/2010. V.M.L. acknowledges partial support from the European FP7 program by SIMTECH, Grant No. 246937, from The Science and Technology Center in Ukraine, by the Grant No. 5716-2, “Development of Graphene Technologies,” and from the Special Program of Fundamental Researches of the NAS of Ukraine.

APPENDIX

In calculation of the interaction function, Eq. (15), the essential task consists in the integration as follows:

$$\frac{1}{2N} \sum_{\mathbf{k}} e^{i\mathbf{k}\cdot\mathbf{n}} (G_{\mathbf{k}}^{(0)})_{jj} = \frac{2 \cos \mathbf{K} \cdot \mathbf{n}}{W^2} \int_0^W J_0\left(\frac{\xi n}{\hbar v_F}\right) \times \frac{(N_j(\varepsilon) - \xi^2) \xi d\xi}{(\xi^2 - \xi_1^2)(\xi^2 - \xi_2^2)}, \quad (\text{A1})$$

where J_0 is the zeroth-order Bessel function, $\xi_{1,2}^2 = \varepsilon^2 + \varepsilon_2^2 \pm \delta^2(\varepsilon)$ are the complex poles of $\det \hat{G}_{\mathbf{k}}^{(0)}$ in ξ variable, and all $|N_j(\varepsilon)| \sim \varepsilon_g^2$ [as seen from Eq. (6)]. Since this integral is fast converging after $\xi \gtrsim \varepsilon_g$, its upper limit can be safely extended to infinity. Then, after expanding the factor besides the Bessel function in simple fractions,

$$\frac{N_j(\varepsilon, \xi)}{(\xi^2 - \xi_1^2)(\xi^2 - \xi_2^2)} = \frac{N_j(\varepsilon) - \xi_1^2}{\xi^2 - \xi_1^2} - \frac{N_j(\varepsilon) - \xi_2^2}{\xi^2 - \xi_2^2}, \quad (\text{A2})$$

the Hankel-Nicholson integration formula can be applied to each of them:

$$\int_0^\infty \frac{J_0(x)xdx}{x^2 + z^2} = K_0(z), \quad (\text{A3})$$

with the zeroth-order Macdonald function K_0 , valid for complex z if $\text{Re}z > 0$ (Ref. [43]). The z arguments related to the terms in Eq. (A2) can be defined as $z_{1,2}^2 = -\xi_{1,2}^2(n/\hbar v_F)^2$ and the above requirement will read $\text{Re}\sqrt{-\xi_{1,2}^2} > 0$. For the

relevant energy range $0 < \varepsilon_g - \varepsilon \ll \varepsilon_g$, we can use the choices $\sqrt{-\xi_{1,2}^2} = \sqrt{\delta^2(\varepsilon) - \varepsilon^2 - \varepsilon_g^2} \mp i\sqrt{\delta^2(\varepsilon) + \varepsilon^2 + \varepsilon_g^2}$. At last, for relevant distances $n \gtrsim r_0$, the resulting $K_0(z_{1,2})$ have big enough arguments, $|z_{1,2}| = |n\xi_{1,2}/\hbar v_F| \gtrsim 1$, to use their asymptotics: $K_0(z_1) \approx -\sqrt{2/\pi z_1}e^{-z_1}$ and $K_0(z_2) \approx \sqrt{2/\pi z_2}e^{-z_2}$. Then, taking account of all prefactors besides these expressions present in Eqs. (15) and (A2), we arrive at the final result of Eq. (15).

-
- [1] K. S. Novoselov, A. K. Geim, S. V. Morozov, D. Jaing, Y. Zhang, S. V. Dubonos, I. V. Grigorieva, and A. A. Firsov, *Science* **306**, 666 (2004).
- [2] P. R. Wallace, *Phys. Rev.* **71**, 622 (1947).
- [3] G. W. Semenoff, *Phys. Rev. Lett.* **53**, 2449 (1984).
- [4] K. S. Novoselov, E. McCann, S. V. Morozov, V. I. Fal'ko, M. I. Katsnelson, U. Zeitler, D. Jiang, F. Schedin, and A. K. Geim, *Nature Phys.* **2**, 177 (2006).
- [5] Y. Zhang, Y.-W. Tan, H. L. Störmer, and P. Kim, *Nature (London)* **438**, 201 (2005); Y. Zhang, T.-T. Tang, C. Girit, Z. Hao, M. C. Martin, A. Zettl, M. F. Crommie, Y. R. Shen, and F. Wang, *ibid.* **459**, 820 (2009).
- [6] E. McCann, *Phys. Rev. B* **74**, 161403 (2006).
- [7] E. V. Castro, K. S. Novoselov, S. V. Morozov, N. M. R. Peres, J. M. B. Lopes dos Santos, J. Nilsson, F. Guinea, A. K. Geim, and A. H. Castro Neto, *Phys. Rev. Lett.* **99**, 216802 (2007).
- [8] T. Ando and M. Koshino, *J. Phys. Soc. Japan* **78**, 034709 (2009).
- [9] J. D. Bernal, *Proc. R. Soc. London, Ser. A* **106**, 749 (1924).
- [10] W. Tao, G. Qing, L. Yan, and S. Kuang, *Chinese Phys. B* **21**, 067301 (2012).
- [11] J. Liu and W. Zhang, *RSC Adv.* **3**, 21943 (2013).
- [12] R. M. Ribeiro and N. M. R. Peres, *Phys. Rev. B* **83**, 235312 (2011).
- [13] J. Slawinska, I. Zasada, and Z. Klusek, *Phys. Rev. B* **81**, 155433 (2010).
- [14] A. Ramasubramaniam, D. Naveh, and E. Towe, *Phys. Rev. B* **84**, 205325 (2011).
- [15] S. M. Sze, *Physics of Semiconductor Devices* (Wiley, New York, 1969).
- [16] B. I. Shklovskii and A. L. Efros, *Electronic Properties of Doped Semiconductors* (Springer-Verlag, Berlin, 1984).
- [17] J. Nilsson and A. H. Castro Neto, *Phys. Rev. Lett.* **98**, 126801 (2007).
- [18] A. Feher, E. Syrkin, S. Feodosyev, I. Gospodarev, E. Manzhelii, A. Kotlar, and K. Kravchenko, in *Nanotechnology and Nanomaterials, New Progress on Graphene Research*, edited by Jian Ru Gong (InTech, Rijeka, 2013), Chap. 5.
- [19] M. A. Ivanov and Y. G. Pogorelov, *Sov. Phys. JETP* **61**, 1033 (1985).
- [20] Y. Zhang, A. Mascarenhas, H. P. Xin, and C. W. Tu, *Phys. Rev. B* **61**, 7479 (2000).
- [21] N. F. Mott, *Adv. Phys.* **16**, 49 (1967).
- [22] M. A. Ivanov, V. M. Loktev, and Y. G. Pogorelov, *Phys. Rep.* **153**, 209 (1987).
- [23] V. L. Bonch-Bruевич and S. V. Tyablikov, *The Green Function Method in Statistical Mechanics* (North-Holland, Amsterdam, 1962).
- [24] E. N. Economou, *Green's Functions in Quantum Physics* (Springer, New York, 2006), p. 87.
- [25] P. T. Araujo, M. Terrones, and M. S. Dresselhaus, *Mater. Today* **15**, 98 (2012).
- [26] I. M. Lifshitz, S. A. Gredeskul, and L. A. Pastur, *Introduction to the Theory of Disordered Systems* (Wiley, New York, 1988).
- [27] C. Bena, *Phys. Rev. Lett.* **100**, 076601 (2008).
- [28] J. Nilsson, A. H. Castro Neto, F. Guinea, and N. M. R. Peres, *Phys. Rev. B* **78**, 045405 (2008).
- [29] H. P. Dahal, A. V. Balatsky, and J.-X. Zhu, *Phys. Rev. B* **77**, 115114 (2008).
- [30] P. W. Anderson, *Phys. Rev.* **109**, 1492 (1958).
- [31] D. N. Sheng, L. Sheng, and Z. Y. Weng, *Phys. Rev. B* **73**, 233406 (2006).
- [32] P. W. Anderson, *Phys. Rev.* **124**, 41 (1961).
- [33] R. R. Biswas, S. Sachdev, and D. T. Son, *Phys. Rev. B* **76**, 205122 (2007).
- [34] V. M. Pereira, V. N. Kotov, and A. H. Castro Neto, *Phys. Rev. B* **78**, 085101 (2008).
- [35] Y. G. Pogorelov, M. C. Santos, and V. M. Loktev, *Phys. Rev. B* **84**, 144510 (2011); **88**, 224518 (2013).
- [36] P. Soven, *Phys. Rev.* **156**, 809 (1967).
- [37] R. J. Elliott, J. A. Krumhansl, and P. L. Leath, *Rev. Mod. Phys.* **46**, 465 (1974).
- [38] A. F. Ioffe and A. R. Regel, *Progr. Semicond.* **4**, 237 (1960).
- [39] K. Carva, B. Sanyal, J. Fransson, and O. Eriksson, *Phys. Rev. B* **81**, 245405 (2010).
- [40] A. V. Zayats, I. I. Smolyaninov, and A. A. Maradudin, *Phys. Rep.* **408**, 131 (2005).
- [41] V. V. Mkhitarian and E. G. Mishchenko, *Phys. Rev. Lett.* **110**, 086805 (2013).
- [42] Z. Ni, Q. Liu, K. Tang, J. Zheng, J. Zhou, R. Qin, Z. Gao, D. Yu, and J. Lu, *Nano Lett.* **12**, 113 (2012).
- [43] M. Abramowitz, I. Stegun. *Handbook of Mathematical Functions: with Formulas, Graphs, and Mathematical Tables*, Washington: National Bureau of Standards (1972), p. 488.